Granular Avalanches in Fluids

Sylvain Courrech du Pont,[1] Philippe Gondret,[1] Bernard Perrin,[2] and Marc Rabaud[1]

[1]*Laboratoire Fluides, Automatique, Systèmes Thermiques (UMR CNRS 7608), Bâtiment 502, Campus Universitaire,
91405 Orsay cedex, France*
[2]*Laboratoire de Physique de la Matière Condensée (UMR CNRS 8551), 24, rue Lhomond, 75231 Paris cedex, France*
(Received 25 July 2002; published 28 January 2003)

Three regimes of granular avalanches in fluids are put in light depending on the Stokes number St which prescribes the relative importance of grain inertia and fluid viscous effects and on the grain/fluid density ratio r. In gas ($r \gg 1$ and St > 1, e.g., the dry case), the amplitude and time duration of avalanches do not depend on any fluid effect. In liquids ($r \sim 1$), for decreasing St, the amplitude decreases and the time duration increases, exploring an inertial regime and a viscous regime. These three regimes are described by the analysis of the elementary motion of one grain.

Granular matter has received much attention from physicists over the past few years [1]. Beyond the fundamental interest in the physics of granular systems which can present some features of either solids, liquids, or even gases, the understanding of granular materials is important in many industrial activities such as pharmacology, chemical engineering, and the cereal industry, but also in environmental problems such as dune migration, sediment transport, landslides, and avalanches. Avalanches observed when building a pile start at the maximum angle of stability θ_m and stop at the angle of repose $\theta_r < \theta_m$. Most studies concern dry avalanches where the ambient air is inoperative for the pile stability and the avalanche dynamics [2–4] except in fine cohesive dry powders [5]. In wet granular materials, recent studies show that the adhesive forces caused by capillary bridges between grains strongly affect the pile stability and dynamics [6]. But to date no detailed study has focused on the influence of the interstitial fluid for a totally immersed grain assembly. This influence is certainly important in granular avalanche processes, as evidenced by the marked differences between the propagation of subaqueous and eolian dunes: Even if the slope angles are quite similar, the flow is generally continuous in the lee side of a submarine dune, but occurs by successive avalanches in the dry case [7]. This observation prompted geologists to accumulate data on avalanches of sand or beads in rotating drums filled with air or water [8] or even with glycerol mixtures [9], which seemed to show that the amplitude of avalanches decreases and the time duration increases with the fluid viscosity.

We have performed an extensive series of experiments to investigate the influence of the interstitial fluid on the packing stability and the avalanche dynamics. The analysis of our results obtained with a rotating drum setup indicate the existence of three regimes: (i) a free-fall regime for which there is no fluid influence and that corresponds to the classical dry regime, and two regimes where the interstitial fluid governs the avalanche

dynamics, namely, (ii) a viscous and (iii) an inertial regime.

Our rotating drum consists of a cylinder of inner diameter D ranging from 8 to 46 cm and lying on two parallel rotation axes. It is driven by a microstep motor followed by a 1/100 reducer and a rubber transmission so that the cylinder turns at the rotation rate Ω by steps of 10^{-3} degree without shocks. The cylinder is half filled with sieved solid spheres of diameter d and density ρ_s, totally immersed in a fluid of density ρ_f and dynamic viscosity η. The pile is confined between two parallel glass end walls with a sufficiently large gap width b ($b/d > 15$) to avoid wall effect [10]. This study was achieved at low enough rotation rate Ω ($\sim 10^{-5}$ rpm) to be in the intermittent regime of macroscopic avalanches [3]: The pile slope increases linearly with time at the rate Ω and then quickly relaxes by a surface avalanche process. With a CCD camera aligned along the cylinder axis, images are taken at regular time intervals and analyzed to track the pile interface. Except during the avalanches, the interface is found to be linear, with a roughness of the order of 1 grain size, which justifies the calculation of the averaged slope angle θ of the pile with the resolution 0.01°.

Two typical recordings for the time evolution of the average slope angle θ are displayed in Fig. 1 for 230 μm glass beads immersed either in air or water. We focus on two typical parameters of the avalanche dynamics that we found uncorrelated: The avalanche amplitude characterized by the hysteresis angle $\Delta\theta = \theta_m - \theta_r$ and the avalanche time duration T, which is calculated as the time interval between 5% and 95% of the corresponding avalanche amplitude. The mean values $\overline{\Delta\theta}$ and $\overline{T}$ are then calculated for one experiment over all the successive macroscopic avalanches that affect the entire slope. In the following, we drop the mean bar notations for simplicity. Two different behaviors clearly appear: In the air case [Fig. 1(a)], the avalanche amplitude $\Delta\theta$ is large (few degrees) and the avalanche duration T is small (~ 1 s),
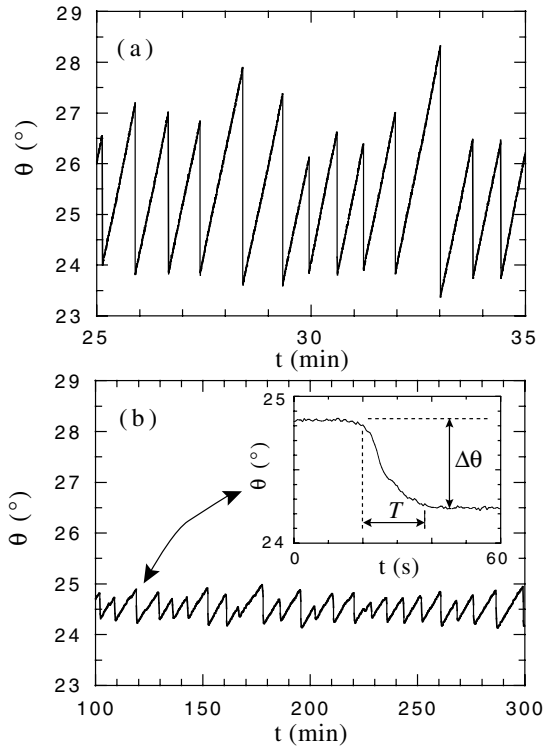
FIG. 1. Time evolution of the slope angle θ of a pile of glass beads ($d = 230 \pm 30$ μm) immersed in (a) air or (b) water and contained in a rotating drum. The inset is a zoom of an avalanche in the water case.
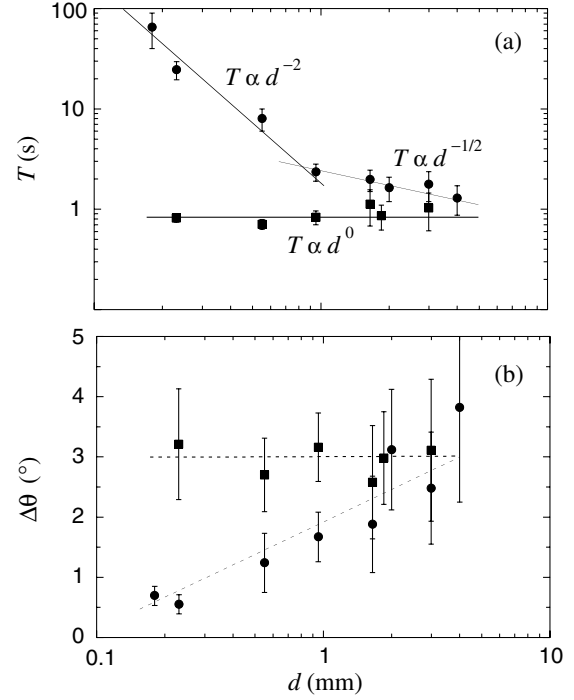

FIG. 2. Time duration T and amplitude $\Delta\theta$ of macroscopic avalanches as a function of the grain diameter d for glass beads immersed in air (■) or water (●) in a rotating cylinder of diameter $D = 16$ cm. The error bars correspond to the standard deviation.

whereas in the water case [Fig. 1(b)], $\Delta\theta$ is small (less than 1°) and T is large (~ 1 min). One crucial parameter of the phenomenon appears to be the particle diameter d when one looks in Fig. 2 at the evolution of T and $\Delta\theta$ as a function of d when the grains are immersed either in air or in water. In the air case, there is no significant dependency of T and $\Delta\theta$ on d. By contrast, in the water case, the avalanche duration which is close to the air case for the larger d, increases first slightly ($T \propto d^{-1/2}$), then drastically ($T \propto d^{-2}$) from typically 2 to 100 s when the grain size is decreased from 1 to 0.18 mm. In parallel, the avalanche amplitude $\Delta\theta$ in water decreases from the air value for the larger d close to zero when the grain size is decreased to 0.18 mm.

The pertinent dimensionless parameters governing the avalanche dynamics in fluids can be inferred by considering the elementary falling process of one solid grain on its neighbor from below in a fluid and under the action of gravity. Let us write the simplified following equation of motion for the grain of velocity u down the slope between two collisions:

$$\frac{\pi}{6}\rho_s d^3 \frac{du}{dt} = \frac{\pi}{6}\Delta\rho g d^3 \sin\theta - F_d. \qquad (1)$$

Starting from zero velocity, the grain increases its grain momentum at the rate $(\pi/6)\rho_s d^3 (du/dt)$ under the action of its apparent weight $(\pi/6)\Delta\rho g d^3 \sin\theta$ (where $\Delta\rho = \rho_s - \rho_f$) minus a fluid drag force F_d. At

this basic stage, the solid friction force can be modeled by a dynamical Coulombic term which just reduces the apparent gravity. Two behaviors can be discussed according to the value of the particle Reynolds number Re: At Re $\ll 1$, F_d is equal to the viscous Stokes force $3\pi d\eta u$ so the grain will possibly reach its viscous limit velocity $U_{\infty v} = \Delta\rho g d^2 \sin\theta/18\eta$ in the characteristic time $\tau_{cv} = \rho_s d^2/18\eta$, i.e., for a characteristic distance $\delta_{cv} = \tau_{cv} U_{\infty v}$. At Re $\gg 1$, F_d is the inertial fluid force $C_d(\pi/6)d^2\rho_f u^2$, and the corresponding inertial characteristic time and distance are $\tau_{ci} = (\rho_s/\rho_f)^{1/2}(2\rho_s d/\Delta\rho g \sin\theta)^{1/2}$ and $\delta_{ci} = \tau_{ci} U_{\infty i}$, where $U_{\infty i} = (2\Delta\rho g d \sin\theta/\rho_f)^{1/2}$ is the inertial limit velocity (for simplicity, we take here the drag coefficient as constant: $C_d \simeq 1/\pi \simeq 0.3$). By comparing the two characteristic distances δ_{cv} and δ_{ci} with the elementary distance between two successive collisions taken as the grain diameter d, we introduce two dimensionless numbers, St and r, which govern the grain dynamics in this elementary falling process: $\delta_{cv}/d = 2(\tau_{cv}/\tau_{ff})^2 = 2\mathrm{St}^2$ and $\delta_{ci}/d = 2(\tau_{ci}/\tau_{ff})^2 = 2r^2$, where $\tau_{ff} = (2\rho_s d/\Delta\rho g \sin\theta)^{1/2}$ is the typical time scale of free falling of a grain over d, St $= (1/18\sqrt{2})\rho_s^{1/2}(\Delta\rho g \sin\theta)^{1/2}d^{3/2}/\eta$ is the Stokes number which prescribes the relative importance of grain inertia and fluid viscous effects, and $r = (\rho_s/\rho_f)^{1/2}$ is related to the density ratio. For St $\gg 1$ and $r \gg 1$, the grain does not reach any limit regime over d: This is the "free-fall

regime." For St $\ll 1$ and $r \gg 1$, the grain reaches its limiting Stokes velocity: This is the "viscous limit regime." For St $\gg 1$ and $r \ll 1$, the grain reaches its limiting inertial velocity: This is the "inertial limit regime." For St $\ll 1$ and $r \ll 1$, the grain reaches one limit velocity depending on the particle Reynolds number Re $= \tau_{cv}/\tau_{ci} = St/r$: for Re $\ll 1$ (Re $\gg 1$) the limit regime is the viscous (inertial) one. The exact boundaries between the three domains in the (St, r) plane of Fig. 3 will be precised further. In this diagram are reported all experiments (ours and others [4,9]) corresponding to different sphere materials (glass, steel, and nylon) in different fluids (air, water, silicone oils, or glycerol mixtures of different viscosities). They correspond to roughly two lines in this diagram: one line for the liquid case where $r \sim 1$ and St ranges from 0.2 to 40 and another line for the air case where $r \sim 40$ and St ranges from 30 to 10^4.

Let us now look if the complex dynamics of macroscopic granular avalanches in fluids can be related to these elementary falling processes. In the two limit regimes, one may reasonably suppose that the time duration T of a macroscopic granular avalanche will scale as D/d elementary falls, each of time duration d/U_∞, so that $T_v = D/U_{\infty v} = 18\eta D/\Delta\rho g d^2 \sin\theta$ in the viscous limit regime and $T_i = D/U_{\infty i} = D\rho_f^{1/2}/(2\Delta\rho g d \sin\theta)^{1/2}$ in the inertial limit regime. These scalings correspond to the d dependence observed in Fig. 2: $T \propto d^{-2}$ and $T \propto d^{-1/2}$ for small and large d, respectively. The plots of T/T_v and T/T_i show clearly the existence of a viscous regime characterized by the plateau $T/T_v \simeq 4$ for St $\lesssim 4$ [Fig. 4(a)] and an inertial regime characterized by the plateau $T/T_i \simeq 2$ for St $\gtrsim 4$ [Fig. 4(b)]. A careful analysis of each data point allows us to identify the critical Reynolds number Re$_c \simeq 2.5$ for the viscous/inertial tran-
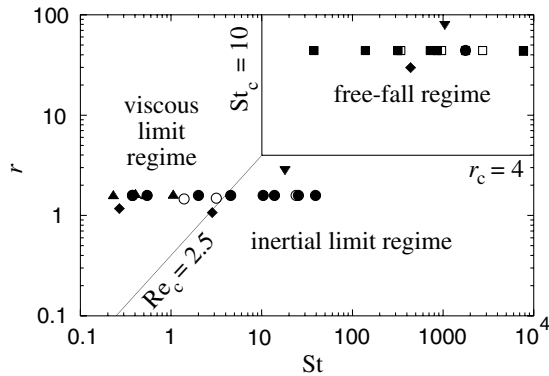
sition corresponding to the boundary line of slope 1 in the log-log plane (St, r) of Fig. 3.

In the elementary free-fall regime (St $\gg 1$ and $r \gg 1$), a succession of elementary falling processes would lead to the avalanche time duration $T = (D/d)\tau_{ff} = D(2\rho_s/\Delta\rho g d \sin\theta)^{1/2}$, which is not consistent with the non-d dependence observed in Fig. 2. In addition, we have observed that T scales as $D^{1/2}$ in the air case rather than as D. These observations lead us to consider a dry avalanche as a global accelerated rush over D of macroscopic time scale $T_{ff} = (2\rho_s D/\Delta\rho g \sin\theta)^{1/2}$. This scaling is indeed observed as all data in air collapse onto the plateau $T \simeq 3T_{ff}$ for St $\gtrsim 30$ [Fig. 4(c)]. In all three regimes, the plateau values of Figs. 4(a)–4(c) are not far from one, meaning that our crude approach catches the essential of the avalanche dynamics in fluids.

Let us focus now on the avalanche amplitude $\Delta\theta$. The plot of $\Delta\theta$ as a function of St (Fig. 5) shows two behaviors. At large St (St $\gtrsim 20$), $\Delta\theta$ has the constant value $\Delta\theta \simeq 3^o \pm 1^o$ whereas $\Delta\theta$ clearly decreases with St at small St (St $\lesssim 20$). We also observe that the decrease of $\Delta\theta$ at small St is essentially due to a decrease of the maximum angle of stability θ_m (cf. Fig. 1). Let us recall that the Stokes number is the only parameter that governs the coefficient of restitution e for an immersed binary collision between solid grains [11]: Under the critical value
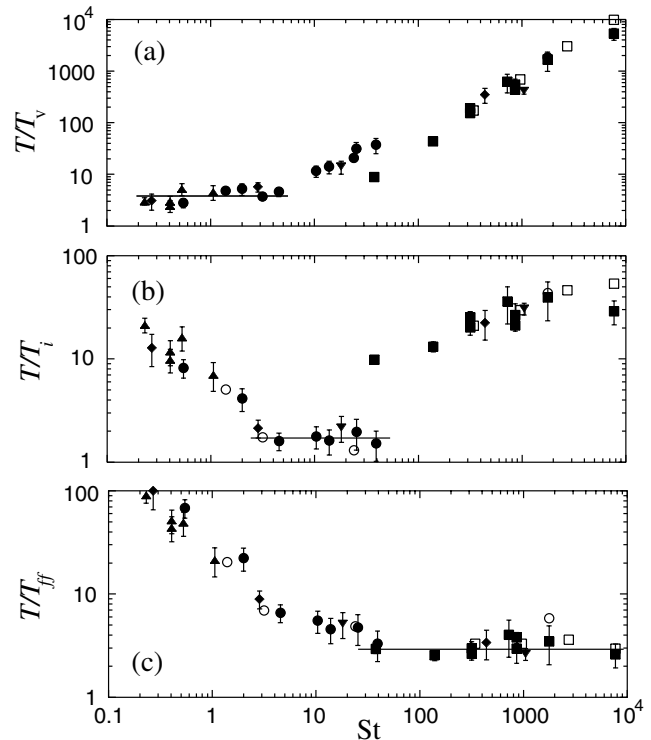
FIG. 3. Diagram of the different regimes for the elementary falling process of one grain in the (St, r) plane. Our results (filled symbols) correspond to glass beads in air (■) or water (●), or in silicone oils of viscosity 5, 10, or 20 Pa s (▲), to nylon spheres (◆) in air, water, and silicone oil (2 Pa s), and to steel spheres in air and water (▼). Other results (open symbols) of Evesque [4] (□) and Allen [9] (○) correspond to glass beads in air and different water-glycerol mixtures.

FIG. 4. Time duration T of macroscopic avalanches normalized either by (a) the viscous time scale T_v (b) the inertial time scale T_i or (c) the free-fall time scale T_{ff} as a function of the Stokes number St for different grains in different fluids and rotating cylinders of different diameter D. Same symbols as in Fig. 3.
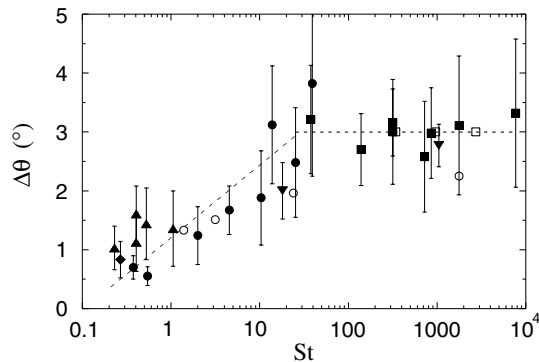
FIG. 5. Amplitude $\Delta\theta$ of macroscopic avalanches as a function of the Stokes number St. Same symbols as in Fig. 3.

$St_c \simeq 10$, $e = 0$, the collision is totally inelastic as all the kinetic energy of the grain is dissipated by the fluid during the collision process. Above St_c, e increases quickly with St and becomes close to its maximal "dry" value ($\simeq 1$) for $St \gtrsim 100$. It is worth noting that the curve $e = f(St)$ is the same whatever the density ratio r [11]. Considering again the immersed granular avalanches in fluids, the grain kinetic energy will be totally dissipated by the fluid in the collision process at low St, with an all the more smooth collision when St evolves towards zero. The obtained packing is thus certainly all the more loose [12], leading to a lower maximum angle of stability [13] and explaining the decrease of $\Delta\theta$ with St at low St.

In addition, if one consider the critical Stokes value $St_c \simeq 10$ independent of r as the boundary line between the accelerated regime and viscous limit regime in the (St, r) plane of Fig. 3, this leads to the critical density ratio $r_c = St_c/Re_c \simeq 4$ separating the free-fall regime and the inertial limit regime. As r values larger than 4 ($\rho_s/\rho_f > 16$) can hardly be reached experimentally for solid/liquid systems, the free-fall regime corresponds only to solid/gas systems such as, e.g., the dry granular avalanches.

Finally, we observe for large St ($St \gtrsim 20$) that all occurring events are macroscopic avalanches that affect the entire slope: The size distribution is a Gaussian curve centered on the value $\Delta\theta \simeq 3°$. This kind of distribution, classically found for weakly dissipative dry granular avalanches [2–4], is incommensurate with the ideas of self-organized criticality (SOC) which predict a power law distribution without any typical scale as found in strongly overdamped cellular automata (CA) [14]. These two limit behaviors can be brought together by introducing some inertia in CA [15] or more dissipation in granular systems [16]. As suggested in Ref. [17], one way to introduce dissipation is to immerse the grains in a liquid. In our immersed experiments, we indeed observe for decreasing St ($St \lesssim 20$) the appearance of numerous small events (not affecting all the slope) together with the Gaussian distributed large events. Such a behavior

was excepted in the viscous regime of low St as the hysteresis $\Delta\theta$ of the system goes to zero with St, which is a condition for the system to evolve towards criticality. But up to now, we have not enough resolution to characterize the size distribution of these small events and to conclude if it obeys or not the SOC power law.

In conclusion, we have shown the existence of three regimes (free-fall, inertial limit, and viscous limit) for granular avalanches in fluids, controlled by the Stokes number which measures the ratio of particle inertia to viscous fluid effects, and the density ratio. The time duration of the macroscopic avalanches that affect the entire slope has been predicted in all these three regimes by a simple modeling of one grain motion. The amplitude of these macroscopic avalanches, constant at high St, decreases at low St. Finally, more refined experiments remain to be done to see if the system evolves towards criticality when fluid dissipation increases ($St \rightarrow 0$).

[1] H. M. Jaeger, S. R. Nagel, and R. P. Behringer, Rev. Mod. Phys. **68**, 1259 (1996); P.-G. de Gennes, Rev. Mod. Phys. **71**, S374 (1999); J. Duran, *Sand, Powders, and Grains* (Springer, New York, 2000).

[2] P. Evesque and J. Rajchenbach, C. R. Acad. Sci., Ser. II: Mec., Phys., Chim., Sci. Terre Univers **307**, 223 (1988); H. M. Jaeger, C.-H. Liu, and S. R. Nagel, Phys. Rev. Lett. **62**, 40 (1989).

[3] J. Rajchenbach, Phys. Rev. Lett. **65**, 2221 (1990); M. Caponeri *et al.*, in *Mobile Particulate Systems*, edited by E. Guazzelli and L. Oger (Kluwer, Dordrecht, 1994), pp. 331–366.

[4] P. Evesque, Phys. Rev. A **43**, 2720 (1991).

[5] A. Castellanos *et al.*, Phys. Rev. Lett. **82**, 1156 (1999).

[6] P. Tegzes, T. Vicsek, and P. Schiffer, Phys. Rev. Lett. **89**, 094301 (2002), and references therein.

[7] R. E. Hunter, J. Sediment. Petrol. **55**, 886 (1985).

[8] M. A. Carrigy, Sedimentology **14**, 147 (1970).

[9] J. R. L. Allen, J. Geol. **78**, 326 (1970).

[10] S. Courrech du Pont *et al.*, Europhys. Lett. (to be published).

[11] P. Gondret, M. Lance, and L. Petit, Phys. Fluids **14**, 643 (2002).

[12] G. Y. Onoda and E. G. Liniger, Phys. Rev. Lett. **64**, 2727 (1990).

[13] J. R. L. Allen, Geol. Minjbouw **49**, 13 (1970).

[14] P. Bak, C. Tang, and K. Wiesenfeld, Phys. Rev. Lett. **59**, 381 (1987).

[15] C. P. C. Prado and Z. Olami, Phys. Rev. A **45**, 665 (1992).

[16] M. A. S. Quintanilla *et al.*, Phys. Rev. Lett. **87**, 194301 (2001), and references therein.

[17] H. M. Jaeger and S. R. Nagel, Science **255**, 1523 (1992); D. H. Rothman, J. P. Grotzinger, and P. Flemings, J. Sediment. Res., Sect. A **64**, 59 (1994).